International Journal of Biological Macromolecules xxx (xxxx) 144386

Contents lists available at ScienceDirect

International Journal of Biological Macromolecules

journal homepage: www.elsevier.com/locate/ijbiomac

A dual approach with lignin and nanolignin: Reinforcing UV stability and sustainability in PVA matrices

Amanda S.M. de Freitas [a, b, 1], Jéssica S. Rodrigues [b, 1], Lucas V.B. Fré [a], Henrique O.S. Vieira [a], Maria E.S. Nascimento [a], Stefanny F. Amaro [a], Livia S. Emidio [a], Daniele R. de Araujo [c], Anderson F. Sepulveda [c], Daniel Komatsu [d], Vagner R. Botaro [a], Leonardo F. Fraceto [b], Marystela Ferreira [a, *]

[a] Science and Technology Center for Sustainability (CCTS), Federal University of São Carlos (UFSCar), João Leme dos Santos, km 110, 18052-780 Sorocaba, SP, Brazil
[b] Institute of Science and Technology, São Paulo State University (UNESP), Av. Três de Março 511, 18087-180 Sorocaba, SP, Brazil
[c] Department of Biophysics, Federal University of São Paulo (UNIFESP), Rua Três de maio 100, Vila Clementino, CEP 04044-020 São Paulo, SP, Brazil
[d] Post-Graduation Program of Biomaterials and Regenerative Medicine, Surgery Dept., Faculty of Medical and Health Sciences, Pontifical Catholic University of São Paulo (PUC-SP), Rua Joubert Wey, 290, 18030-070 Sorocaba, SP, Brazil

ARTICLE INFO

Keywords:
Lignin fractionation
Lignin nanoparticles
Photoprotection
Agricultural applications

ABSTRACT

Kraft lignin (KL) and its acetic acid-fractionated derivatives were evaluated for their antioxidant and ultraviolet C (UV-C)-absorbing properties to mitigate the photooxidative degradation of polyvinyl alcohol (PVA). PVA films were prepared with 4 % (*w*/w) KL macroparticles - including unfractionated KL and the fractionated forms KL30, KL40, and KL50 - and with 0.4 % (*w*/w) lignin nanoparticles (NP), derived from the same fractions (named NPKL, NP30, NP40, and NP50). All formulations, including the control (pure PVA), were blended with 10 % (w/w) NPK fertilizer (nitrogen-phosphorus-potassium, 10–10-10) and plasticized with glycerol for film casting. After 21 days of UV-C exposure, films containing LNP retained over 90 % transparency, compared to ~70 % for pure PVA. Fourier-transform infrared spectroscopy (FTIR) and differential scanning calorimetry (DSC) confirmed reduced photooxidative and thermal degradation in lignin-containing films, especially those with KL30 and NP30. Biodegradation assays using respirometric CO_2 analysis showed accelerated release for NP30 (up to 90 mg after 20 days), reflecting enhanced microbial activity. Leaching assays demonstrated controlled release of NPK ions over 40 days in films with NP. In mulch film application tests with cherry tomato, PVA + NP30 showed seedling development comparable to commercial mulch and superior to control films. These results confirm the potential of NP as sustainable, multifunctional additives for UV stabilization and controlled nutrient delivery in biodegradable agricultural films.

1. Introduction

For several decades, synthetic polymer-based materials derived from fossil resources, such as plastics, have dominated material production due to their efficiency and low cost. However, the limited biodegradability of these materials has led to substantial environmental concerns [1]. In this context, polyvinyl alcohol (PVA) has gained attention for its unique characteristics, such as biodegradability, water solubility, and low environmental impact [2,3]. PVA, a polymeric matrix, has vast applications in the biomedical, agricultural, optical, energy and sensor sectors [4]. However, despite all the beneficial properties for various applications, materials made exclusively from PVA have some limitations due to their low mechanical, thermal, and photodegradation resistance and high solubility, especially in heated water [5,6]. Introducing stabilizing agents such as lignin into the PVA matrix, especially in film, membrane and emulsion systems, is a promising solution to these problems.

Lignin can improve thermal and mechanical properties and moisture resistance and provide additional functionalities to PVA, such as UV protection and antioxidant effect. The lignin macromolecule has intrinsic UV absorption properties due to its phenolic and ketone groups [7,8]. It can thus act as a “sacrificial molecule”, absorbing part of the

* Corresponding author.
E-mail address: marystela@ufscar.br (M. Ferreira).
[1] These authors contributed equally to the manuscript

https://doi.org/10.1016/j.ijbiomac.2025.144386
Received 28 March 2025; Received in revised form 5 May 2025; Accepted 18 May 2025
0141-8130/

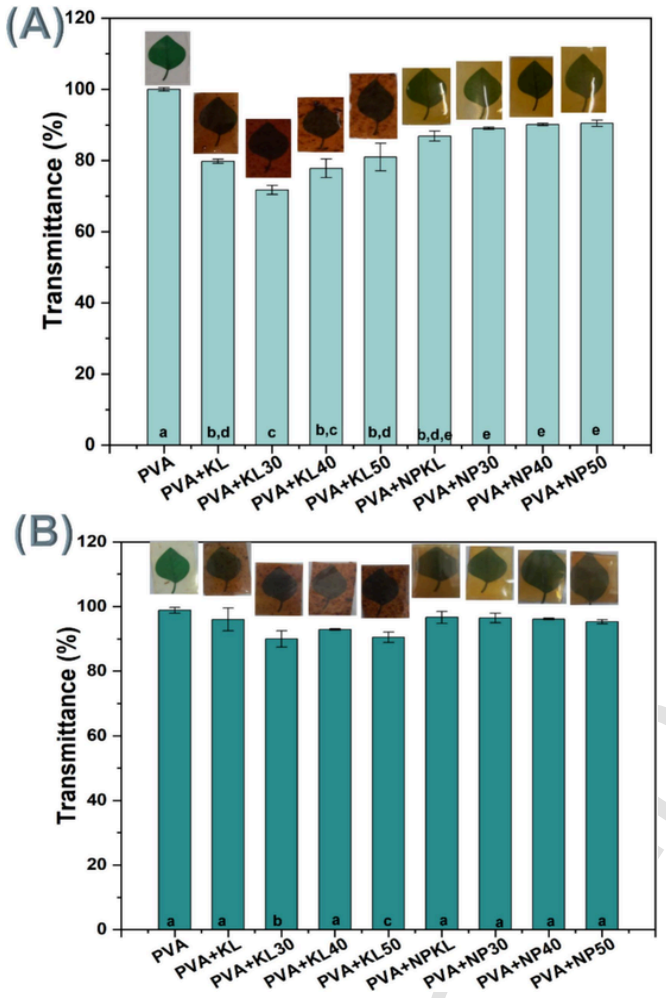

Fig. 1. (A). Initial Transparency and (B) After 21 days, the additive-containing films were analyzed using transmittance measurements. The films include: PVA, PVA + KL, PVA + KL30, PVA + KL40, PVA + KL50, PVA + NPKL, PVA + NP30, PVA + NP40, and PVA + NP50. $^{a\text{-}e}$ Statistically similar samples.

UV light and protecting the polymer matrix from photo-oxidative damage. Recent advances in lignin processing include its fractionation and conversion into lignin nanoparticles (NP). These strategies can modulate the properties of lignin in general, including improving UV blocking efficiency, depending on its structure and molecular size [8,9]. In addition, structural modifications such as sequential fractionation and acetylation can soften its characteristic dark color without compromising its photoprotective capacity, making it a promising alternative to synthetic stabilizers [10].

Fractionating the lignin and reducing its molecular weight has improved UV-blocking properties, while unprocessed lignin shows lower efficiency [11]. Preparing lignin nanoparticles is also a common strategy since lignin NPs generally perform better than their macromolecular counterparts. Studies show increased photoprotective and mechanical properties attributed to lignin's greater surface area and reactivity in NP form, which leads to more effective interactions with the PVA matrix [12].

It is known that understanding the relationship between the molecular structure and properties of lignin is essential to enable the preparation of more stable and durable polymer blends and composites. Thus, lignin, especially in the NP form, can improve UV resistance, modulate other properties, and increase the sustainability of materials. The application of lignin in sectors such as agriculture through plastic mulch films used for weed control and soil moisture retention shows great potential [12]. These polymer films suffer from exposure to the sun, reducing their useful life, due to modifications in their surface, such as loss of color and reduction of mechanical and thermal resistance, which leads to the need to replace these materials in some cases. Incorporating lignin, especially in the NP form, can extend the useful life of these materials, providing an effective barrier against UV irradiation. Previous studies have demonstrated that lignin, when applied in NP form, increases the resistance of materials to photodegradation, proving its efficiency as a natural and renewable UV blocker [8]. Therefore, investigating the structure-performance relationship of different lignin fractions, both in macromolecular and nanoparticle forms, will provide valuable insights for developing more efficient and sustainable polymer composites with broad applications in industry and agriculture. Thus, this study aims to explore and correlate the properties of lignin and its fractions in MP and NP forms and evaluate their performance as UV stabilizers in PVA films, for applications such as mulch film.

2. Materials and methods

2.1. Materials

Lignin was obtained by the precipitation of black liquor from the industrial kraft pulping process of *Eucalyptus urograndis* wood. Acetic acid (CH_3COOH), and acetone (C_3H_6O), were both purchased from Synth®. Poly*v*inyl alcohol (C_2H_4O)x was obtained from Neon, and Anidrol® supplied glycerol ($C_3H_8O_3$). The fertilizer used for film additives was a Mixed Mineral Fertilizer 10–10-10 + micros from Dimy®.

2.2. Sequential fractionation of Kraft lignin in an acidic medium

The fractionation followed the standards of the patent BR 102024 020181 7. In this process, 10 g of KL was added to 100 mL of HOAc solution (10 % *v*/v, with 10 mL HOAc and 90 mL deionized water) and stirred vigorously for 20 min at room temperature (~25 °C). The insoluble lignin was separated by vacuum filtration, dried at 40 °C for 24 h, and then fractionated. HOAc concentrations of 30 %, 40 %, and 50 % were used. Approximately 300 mL of distilled water was added to the filtrate to precipitate the soluble fraction, and each soluble lignin fraction was named KL30, KL40, and KL50 according to the HOAc concentration.

2.3. Lignin nanoparticles synthesis

The antisolvent precipitation method described by Morsali et al. [13] synthesized the NPs. To do this, 0.5 g of dry KL was dissolved in an alcohol solution (30 g of ethyl alcohol and 10 g of deionized water) and stirred for 3 h at room temperature. The solution was filtered through a 0.45 μm membrane (Millipore) to remove the undissolved solids. To form a colloidal dispersion, 120 g of deionized water was added, and the ethyl alcohol was removed using a rotary evaporator at 40 °C under reduced pressure. Based on the fraction, this process was repeated for the KL30, KL40, and KL50 fractions, with the nanoparticles named NPKL, NP30, NP40, and NP50.

2.4. Sample set preparation

Different films were prepared to investigate the structure-performance correlation when using distinct MP lignin fractions and when the NP of these fractions were employed. The solution casting method was used to produce a total of nine additive films. Initially, 11 g of PVA were dissolved in 100 mL of water at 90 °C using a magnetic stirrer until the PVA granules were fully dissolved. Then, 10 mL of glycerol was added as a plasticizer. Next, 4 % (*w*/w with PVA) of KL and its

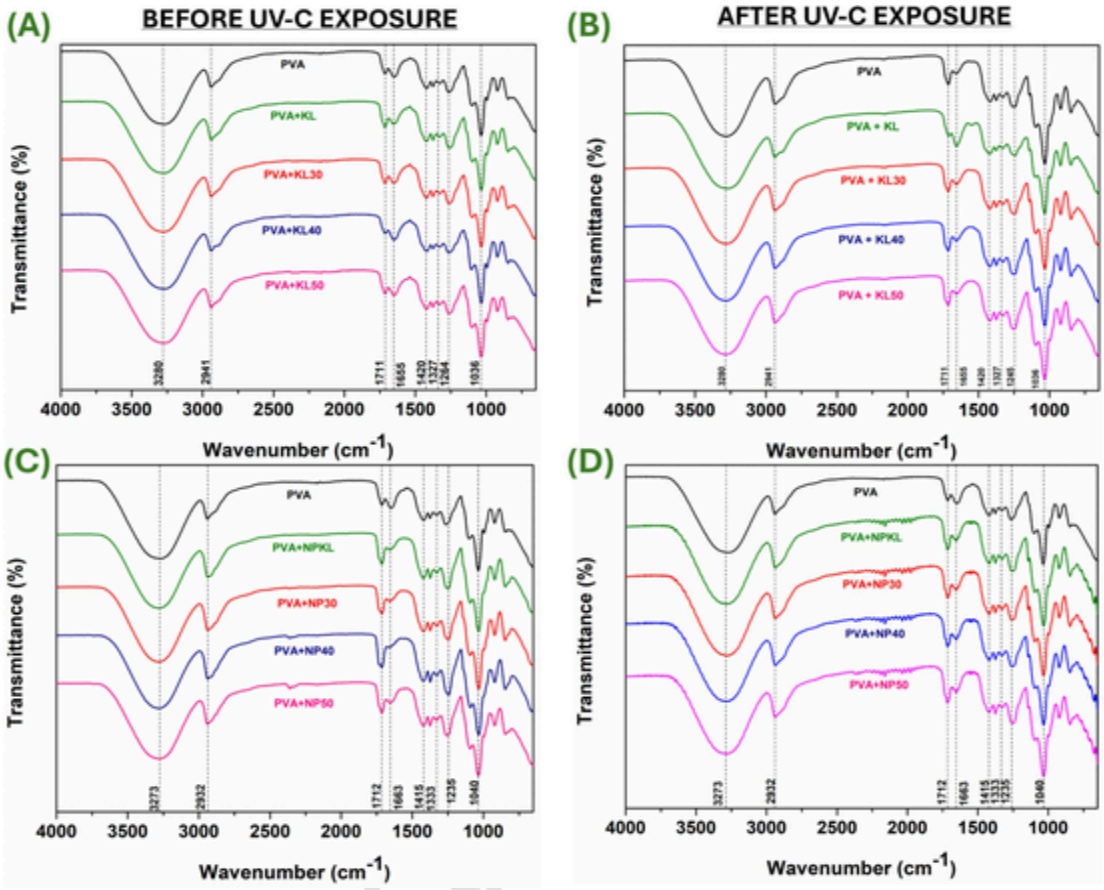

Fig. 2. FTIR spectra of PVA films with additives before (A) and after 21 days of UV-C exposure (B), including KL, KL30, KL40, and KL50. Spectra of films with NP additives before (C) and after 21 days of UV-C exposure (D), including NPKL, NP30, NP40, and NP50.

lignin fractions (KL30, KL40, and KL50) and 10 mL of NPK fertilizer solution were incorporated into the PVA solution and stirred uniformly. The mixture underwent ultrasonication for 30 min to ensure homogeneous dispersion. Afterward, the resulting solution was poured into a mold and dried in an oven at 60 °C under negative pressure (−500 mmHg) for 10 h.

The films were prepared using PVA as the polymer matrix and incorporated either macroparticulate (MP) lignin or lignin nanoparticles (NP). For the MP formulations, one control film containing only PVA (labeled PVA) was prepared, along with four films containing 4 % (*w*/w) of either unfractionated lignin (PVA + KL) or fractionated lignin samples (PVA + KL30, PVA + KL40, and PVA + KL50). In parallel, another set of four films was produced using the same procedure but replacing the 4 % MP lignin with 0.4 % (w/w) of the corresponding lignin NP. These films were labeled PVA + NPKL, PVA + NP30, PVA + NP40, and PVA + NP50, respectively.

2.5. Physical analyses: transparency, moisture content, and solubility

The transparency of the films was measured using UV–Vis spectroscopy by evaluating light transmittance between 200 and 800 nm. Samples were cut uniformly and placed in the spectrophotometer. The percentage of transmitted light indicated the transparency level, showing how MP or NP lignin addition affected the optical properties of the films. The moisture content of the films was determined using a moisture analyzer (A&D Company, model MX-50), following the ABNT NBR 14929:2017 standard. Approximately 1 g of sample was heated at 105 °C until a constant weight was achieved, and the moisture percentage was automatically calculated. Film solubility in phosphate buffer (pH 5, 7, and 9) was determined based on the method of Gontard et al., [14], with some modifications. Cut into 2 × 2 cm squares, films were first dried at 70 °C for 2 h and weighed to determine their dry matter content. They were then immersed in 50 mL of phosphate buffer and kept under slow agitation at room temperature for 24 h. After this period, the solutions were filtered, and the retained material was dried at 70 °C for an additional 24 h and reweighed. The solubility calculation was performed considering the difference in dry mass before and after immersion. The amount of dry matter dissolved in the buffer was determined by subtracting the dry residue's final mass from the dry film's initial mass. The solubility percentage was then calculated based on the initial mass of the film.

2.6. UV-C light exposure

Accelerated aging tests on films were carried out to assess the photodegradation effects of the materials when irradiated with ultraviolet light C (UV-C). UV-C was selected for its high-energy wavelength (254 nm), which is known to induce rapid polymer degradation, including chain scission and oxidation reactions, making it a standard tool for accelerated and comparative stability testing. Although UV-C is not predominant in natural solar radiation, its intense and reproducible action allows for effective screening of the protective performance of additives like lignin under controlled conditions. The tests were conducted in a custom-made photo-aging chamber, where the samples were placed 20 cm from 15 W fluorescent germicidal lamps emitting at 254 nm, with an incident energy of 610 ± 10 μW·cm^{-2}. Samples were exposed

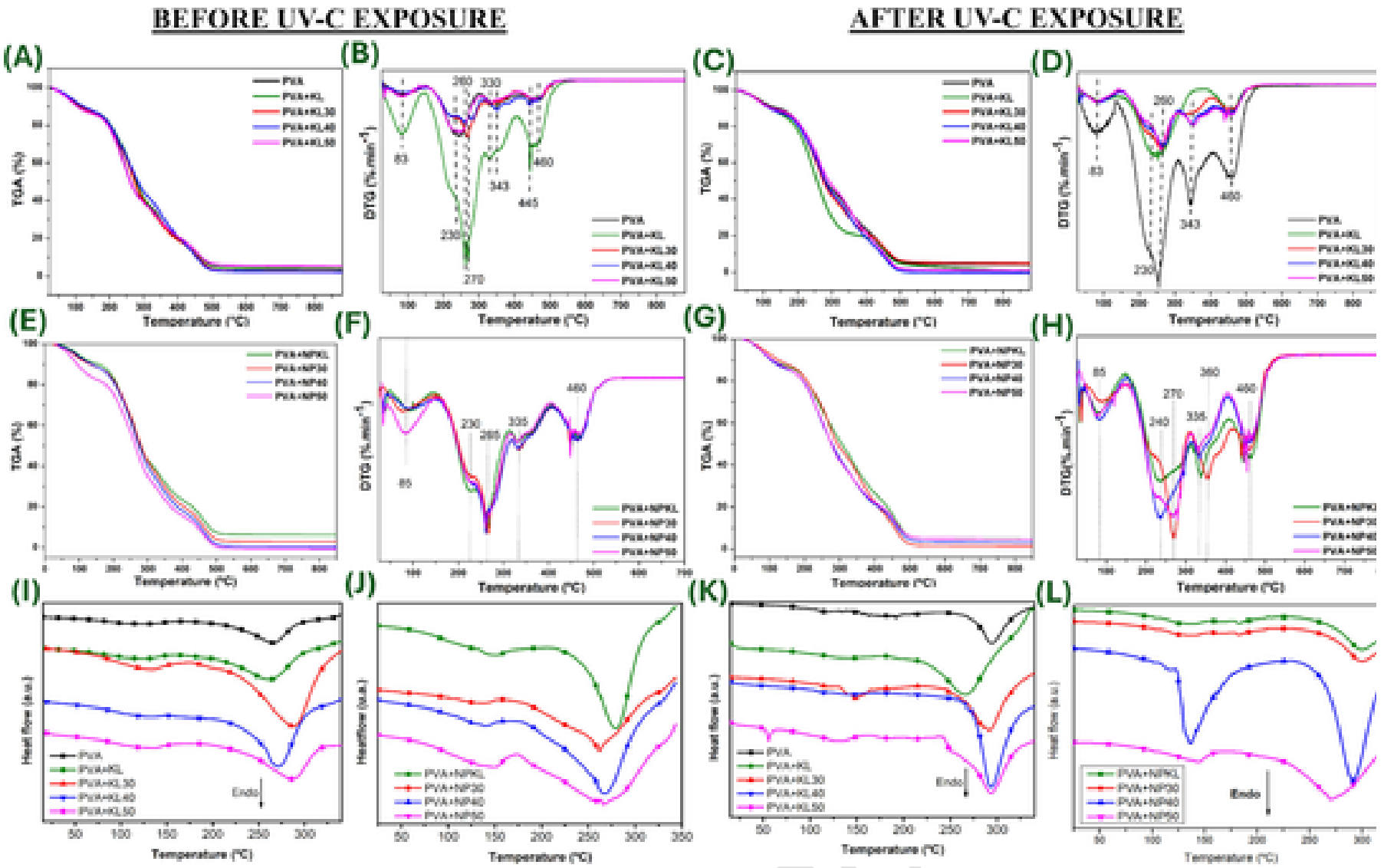

Fig. 3. TG (A, C) and DTG (B, D) curves of each sample based on PVA and lignin fractions variations before (A, B) and after (C, D) exposure to UV-C light. TG (E, G) and DTG (F, H) curves of each sample based on PVA and NP variations before (E, F) and after (G, H) exposure to UV-C light. DSC thermograms of the different treatments: PVA and PVA films additivated with lignin fractions (KL, KL30, KL40, and KL50) (I) and PVA films additivated with NP (J) before exposure to UV-C light; PVA films additivated with lignin fractions (KL, KL30, KL40, and KL50) (K) and PVA films additivated with NP after exposure to UV-C light (L).

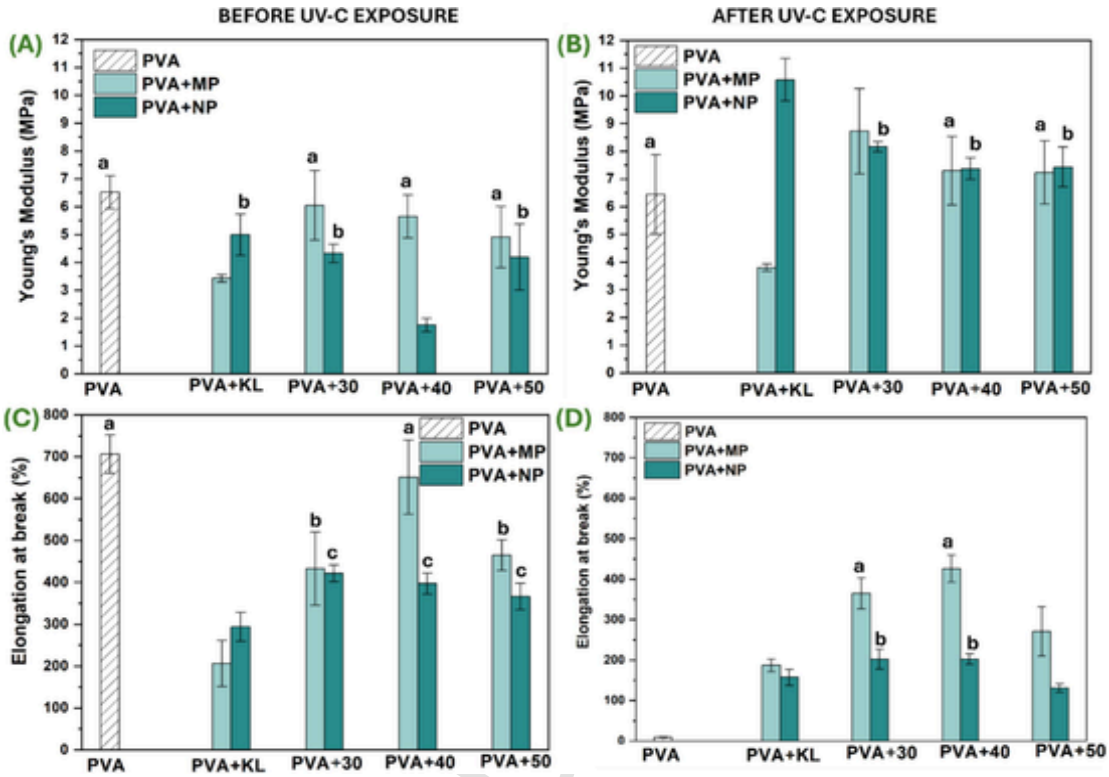

Fig. 4. Mechanical properties of PVA films with the addition of KL, KL30, KL40, and KL50, as well as films containing NP additives: NPKL, NP30, NP40, and NP50. Young's Modulus (MPa) before (A) and after (B) UV-C exposure. Elongation at break (%) before (C) and after (D) UV-C exposure. [a-c]Statistically similar samples.

for 21 days, and their degradation was monitored by FTIR spectroscopy at the beginning and end of the exposure period (0 and 21 days).

2.7. Soil biodegradation

2.7.1. Soil biodegradation study

To evaluate the biodegradation capacity of the films in soil, the 9 prepared compositions were evaluated in triplicate. The films were manually cut into 3 cm squares and buried at a depth of 5 cm in moist soil. During the month of the experiment, the films were unearthed to monitor the evolution of degradation. Photographic records were taken to document the evolution of the process through the condition of the films.

2.7.2. Accelerated biodegradation test

Accelerated biodegradation was analyzed using tests conducted using respirometers (Bartha). In each respirometer, 50 g of soil and 0.5 g of the prepared films were added, totaling 9 respirometers with different films and a control without film. To capture the carbon dioxide (CO_2) released by aerobic microbial activity, 10 mL of 0.2 M KOH solution was added to the side compartment of each respirometer. The KOH solution was collected every 4 days and transferred to an Erlenmeyer flask containing 1 mL of 1 M $BaCl_2$ solution to precipitate the carbonate formed. The excess KOH was then titrated with a standard 0.1 M HCl solution to quantify the CO_2 collected. The KOH solution was replaced in the side compartment after washing with 10 mL of CO_2-free deionized water. The biodegradation process was monitored for 20 days at 28 °C according to ASTM D5988–18 standard (Standard Test Method for Determining Aerobic Biodegradation of Plastic Materials in Soil), with all analyses conducted in triplicate and results compared to controls without any added material.

2.8. Film characterization - before and after UV-C exposure

Fourier-transform infrared spectroscopy (FTIR): The composition of the films was analyzed using an ATR (Attenuated Total Reflectance) accessory in a Nicolet Summit IR 200 spectrometer. Measurements were taken in transmission mode with 126 scans, a nominal resolution of 4.0 cm^{-1}, and 4000 to 400 cm^{-1}. **Thermogravimetric Analysis (TGA):** TGA was performed using a Perkin Elmer Pyris1 TGA with a constant heating rate of 20 °C.min^{-1} up to 900 °C, in an inert nitrogen atmosphere (20 mL.min^{-1} flow). All samples were analyzed in triplicate (n = 3). **Differential Scanning Calorimetry (DSC):** Thermal measurements were conducted with a TA Instruments Q10 DSC, equipped with an RCS 40 cooling system. Samples were initially heated to 100 °C for 5 min to eliminate thermal history, then cooled to −10 °C, followed by a second heating to 350 °C at 20 °C.min^{-1}. All measurements were conducted under a nitrogen flow of 250 mL.min^{-1}, with 4–7 mg sample masses. Each composition was analyzed in triplicate (n = 3). Events were analyzed during the second heating scan using TRIOS® software. **Tensile Testing:** Tensile testing was performed with a Universal Testing Machine (INSTRON EMIC 23–30). Parameters included room temperature (25 °C), a 500 N load cell, and a strain rate of 50 mm min^{-1}. Four specimens per composition were tested at 25 °C according to ASTM D638. Sample dimensions were 70 mm in length, 17 mm in width, and 0.5 mm thickness.

2.9. Rheological analysis

Rheology allows studying the mechanical behavior of viscoelastic materials in different physicochemical conditions through the analysis of rheological parameters obtained by rheometry, such as elastic modulus (G'), viscous modulus (G''), apparent viscosity (η), and shear stress (σ). Measurements were taken using a Malvern Kinexus oscillatory

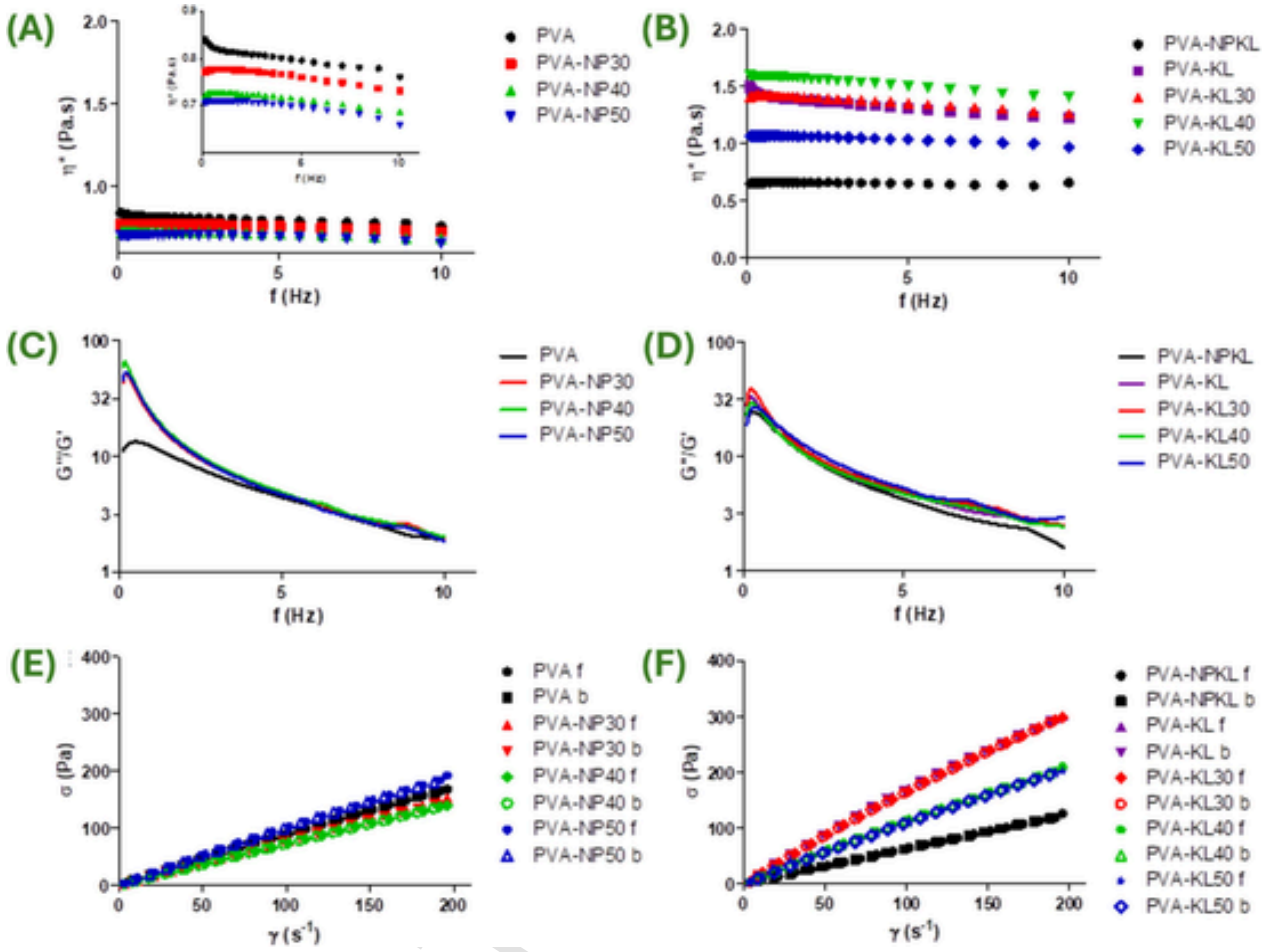

Fig. 5. (A) Apparent viscosity of PVA, PVA-NP30, PVA-NP40, and PVA-NP50 in function of frequency (in Hz) at 25 °C. It is inserted in the same plot but more detailed. (B) Rheogram of apparent viscosity of PVA-NPKL, PVA-KL, PVA-KL30, PVA-KL40, and PVA-KL50 samples in function of frequency (in Hz), at 25 °C. (C) Plot of ratio G"/G' in function of frequency (in Hz) of PVA, PVA-NP30, PVA-NP40, and PVA-NP50, at 25 °C. (D) Plot of ratio G"/G' in function of frequency (in Hz) of PVA-NPKL, PVA-KL, PVA-KL30, PVA-KL40, and PVA-KL50 samples, at 25 °C. (E) Flow curves (shear stress in function of shear rate) of PVA, PVA-NP30, PVA-NP40, and PVA-NP50, at 25 °C. (F) Flow curves of PVA-NPKL, PVA-KL, PVA-KL30, PVA-KL40, and PVA-KL50 samples, at 25 °C. (N = 3).

rheometer, using plate-plate geometry (Ø = 2.5 cm). The interval (or gap) between the geometry and base plates was 0.1 mm. Measurements were taken at 25 °C. Frequency sweeps were carried out to analyze the stability of the materials, with frequencies between 0.1 and 10 Hz. Subsequently, the **G'** data as a function of frequency (**f**) were measured according to the G' power-law model, **S** is the gel strength; **n** is a dimensionless index (Eq. (1)). Analyses were conducted in triplicate (n = 3).

$$G' = S.f^{n} \quad (1)$$

The G' and G" data as a function of frequency were also analyzed by calculating the ratio G"/G', to study the variation in the elasticity of materials as a function of frequency.

The resistance of the materials was also evaluated using a flow curve (or shear stress as a function of increasing and decreasing shear rate), where the materials were subjected to a variation in shear rate γ between 0 and 200 s^{-1}. The forward curves (increase in $\dot{\gamma}$) and backward curves (decrease in $\dot{\gamma}$) were analyzed according to the following power law (Eq. (2)).

$$\sigma = K.\gamma^{m} \quad (2)$$

where K is the consistency index and m the viscosity index (dimensionless). Viscosity curves were also obtained as a function of $\dot{\gamma}$, where the viscosity of the material at $\dot{\gamma} = 0$ can be calculated, that is, the viscosity of the material at rest (η(0)). Measurements were made in triplicate (n = 3). The statistics of the results were performed using One-Way ANOVA, with Tukey's multiple comparison test.

2.10. Evaluation of NPK ion release by leaching

A controlled release test was carried out by leaching the N (NH_4^+), P ($H_2PO_4^-$) and K (K^+) ions present in the fertilizer added to the films. The tests were carried out in triplicate under ambient temperature and humidity conditions, based on the method adapted from Himmah et al. [15]. This methodology seeks to simulate real soil leaching conditions based on film/soil systems. Every week for 40 days, 50 mL of distilled water was poured over the top of the systems, and the leachate was collected. UV–vis spectrophotometry analysis was used to quantify NH_4^+ and $H_2PO_4^-$ ions. A flame photometer was used to measure the release of K^+ ions. Additional details are available in Supporting Information SI1.

2.11. Application of mulch film in cherry tomato cultivation

To test the applicability of the films developed, which showed the best properties for use as mulch, a practical test was carried out using red cherry tomatoes as a model crop for growing cherry tomatoes. The films evaluated included PVA, PVA + KL30, PVA + NP30, a commer-

cial mulch film (control +), and a treatment without any film (control -). For both control samples, the soil was treated with the same volume of NPK fertilizer present in the applied films. The red cherry tomatoes were planted by planting 2 seeds in a 1 cm deep hole per pot containing 150 g of pre-homogenized soil, for each treatment 4 pots were planted. The films for each treatment were cut to cover the top surface of the pot thoroughly and applied immediately after planting the seeds. Throughout the experiment, photographic records of the pots, measurements of the height of the seedlings and the number of leaves were taken weekly to assess the growth, development and effectiveness of the treatment. Plant height measurements and leaf counts were recorded weekly for two months. The health of the plants was also observed, including any signs of nutrient deficiency or stress. Irrigation was carefully controlled to ensure that all the plants received the same amount of water, avoiding variations that could influence the results.

2.12. Statistical data analysis

Statistical analysis was conducted on the numerical data obtained from the analyses to compare result sets and identify significant differences between the studied populations. The one-way ANOVA test was used to compare the means of multiple independent populations. The *p*-value was used to determine statistical significance, with a significance level set at 5 % ($p < 0.05$). For *p*-values below 0.05, a *t*-test was subsequently conducted to evaluate significant differences between pairs of sample sets.

3. Results and discussions

3.1. Chemical functionality of lignin fractions

The fractionation of KL lignin, derived from *Eucalyptus urograndis* wood in acetic acid (HOAc) solution, was detailed by Rodrigues et al. The fractions obtained from KL, called KL30, KL40 and KL50, presented distinct chemical, structural and thermal characteristics. Gel Permeation Chromatography (GPC) analyses revealed that the fractions' weighted average molar mass (Mw) increased with the HOAc concentration. The KL30 and KL40 fractions (1151 and 1446 $g.mol^{-1}$) presented the lowest Mw values, while the KL fraction had the highest Mw of 2653 $g.mol^{-1}$. The KL50 fraction, being intermediate, had an Mw of approximately 1897 $g.mol^{-1}$. Thus, the fractions with the lowest Mw are more soluble in lower concentrations of HOAc, while those with the highest Mw are more soluble in higher acid concentrations.

Regarding the chemical composition, the KL30 fraction exhibited the highest phenolic hydroxyl groups (Ph-OH) content, with 3.47 mmol g^{-1}, followed by the KL40 fraction (2.81 mmol g^{-1}), reflecting its intermediate Mw. On the other hand, the KL and KL50 samples presented higher amounts of aliphatic hydroxyl groups (Aliph-OH), with 1.55 and 1.49 mmol g^{-1}, respectively. The KL30 fraction stood out for its greater free radical scavenging capacity, 76.32 %. The KL40 fraction exhibited intermediate antioxidant activity, lower than KL30 but higher than KL and KL50, in line with its intermediate phenolic content. Knowledge of these differentiated properties between the fractions and the lignin itself will be crucial for understanding the differences that will be found for the films prepared in this study.

3.1.1. Characterization of lignin nanoparticles (NP)

In the previous study, by Rodrigues et al. the characterization of nanoparticles NPKL, NP30, NP40, and NP50 provided key insights into their properties and performance. The NP were morphologically characterized by TEM, which revealed that NPKL particles exhibited heterogeneous morphologies and an average size of 126 nm, suggesting a less controlled synthesis process. In contrast, the nanoparticles prepared with fractionated lignins (NP30, NP40, and NP50) showed predominantly spherical shapes, greater morphological uniformity, and smaller average sizes of approximately 101, 73, and 70 nm, respectively. To complement this analysis, particle size distribution histograms were constructed from the TEM micrographs (Fig. SI2). These histograms confirm a broader size distribution for NPKL, while NPKL30, NPKL40, and NPKL50 presented narrower and more symmetrical distributions, consistent with improved dispersity and more homogeneous particle formation. These results suggest that lignin fractionation contributes to better particle morphology and size control during nanoprecipitation.

The hydrodynamic diameters, obtained by dynamic light scattering (DLS) measurements, corroborated the TEM results, with 251 nm for NPKL and 128, 117, and 106 nm for the samples NP30, NP40, and NP50, respectively. Polydispersity Index (PDI) values ranged from 0.08 to 0.13 for NP30, NP40 and NP50, indicating low polydispersity and consistent particle sizes that contrast with the higher PDI value observed for NPKL. Zeta potential values ranged between −25 and − 31 mV, indicating stable particle dispersions due to electrostatic repulsion, critical to maintaining good dispersion over time. In summary, NP30, NP40, and NP50, derived from fractionated KL, exhibited greater size uniformity, more consistent morphology, and lower PDI values than NPKL. These attributes suggest greater stability and the potential for more controlled applications across various fields. The findings emphasize the significance of selecting appropriate fractions to achieve desired nanoparticle properties and performance.

3.2. Physical properties of additive films

The samples exhibited similar moisture contents: 19.61 ± 1.27 % for PVA, 19.04 ± 0.56 % for PVA + KL, and similar values for KL fractions (18.92 ± 0.91 % to 20.36 ± 1.01 %), with an overall average of 19.04 ± 0.39 %. For the NP-containing samples, moisture values ranged between 17.23 ± 1.30 % and 19.20 ± 0.81 %, with an average of 17.92 ± 1.05 %. There was no statistically significant difference between the two groups, reflecting the uniform amount of water used to produce all films.

The solubility data for films are shown in Fig. SI3. At pH 5, the solubility of the films with different lignin fractions was directly correlated with the Mw of the fractions. Specifically, films with lower M_w exhibited higher solubility, following the KL30 > KL40 > KL50 > KL. For pH levels 7 and 9, solubility remained relatively stable and within the margin of error. This stability can be attributed to the increased solubility of lignin under more alkaline conditions [10], which explains the similar results at pH 7 and 9. All films with additives showed higher solubility than pure PVA, except for PVA + KL50 at pH 5, which behaved similarly to PVA + KL. PVA remains constant across all pH levels, acting as a neutral component that does not influence solubility.

In films with NP, PVA + NP30 showed the highest solubility, exceeding 50 % at all pH levels, with more uniform behavior at pH 7 and 9. PVA + NP40 had intermediate solubility, around 45 % at pH 9, but decreased at pH 5, indicating a more significant influence of alkaline conditions. PVA + NP50 exhibited the lowest solubility (30 %–35 %), with slight variation across pH levels, indicating greater stability. The PVA + NPKL combination had 40 % and 45 % solubility, reinforcing its stability. Due to better nanoparticle dispersion in neutral and alkaline solutions, incorporating lignin nanoparticles increased the films' solubility, particularly at pH 7 and 9. Studies suggest that PVA films with lignin nanoparticles improve solubility and offer UV protection, depending on preparation conditions and nanoparticle size [16].

In Fig. 1A, pure PVA films show the highest transparency, near 100 %, and are ideal for applications like packaging. Adding KL reduces transparency due to its natural opacity, with higher KL concentrations (PVA + KL30, PVA + KL40, PVA + KL50) leading to further reductions. However, films with lignin NP maintain higher transparency (90–100 %) due to better NP dispersion, which minimizes light scattering and maintains clarity. Additionally, the smaller particle size of NP contributes to reduced opacity compared to larger KL particles. This

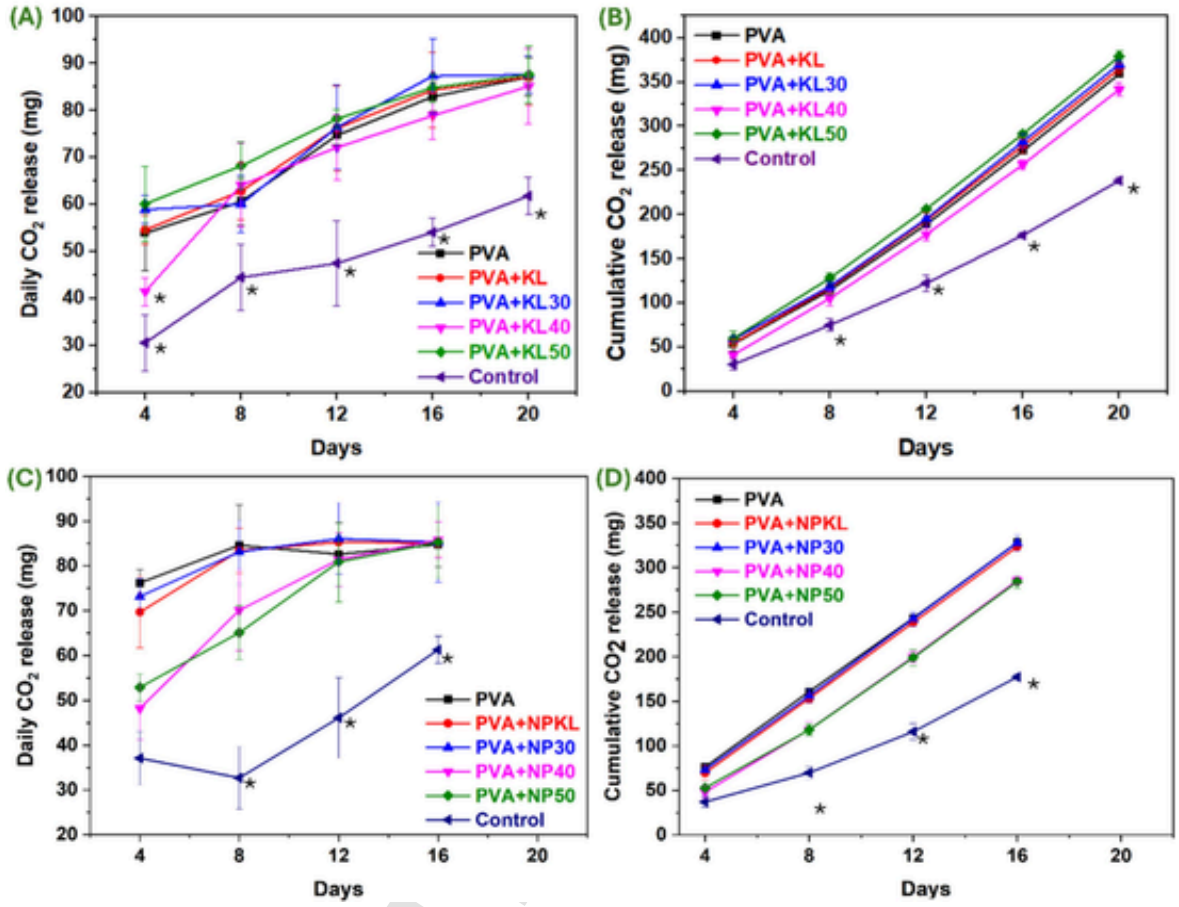

Fig. 6. Biodegradation performance in soil of the samples PVA, PVA + KL, PVA + KL30, PVA + KL40 and PVA + KL50, (A) daily and (B) cumulative CO_2 release. PVA, PVA + NPKL, PVA + NP30, PVA + NP40 and PVA + NP50, (C) daily and (D) cumulative CO_2 release. *Statistically distinct samples from the sample set for the same day interval.

balance between transparency and UV protection highlights the dual role of lignin [17].

Fig. 1B presents the transparency analysis data of the films after 21 days of photodegradation. The PVA film exhibited a significant decrease in transparency to approximately 70 %, indicating that UV exposure compromised its optical properties. In contrast, all films incorporating lignin and lignin nanoparticles-maintained transparencies above 90 %. Statistical analysis reveals that only the PVA + KL30 and PVA + KL50 films showed significantly different transparencies from the other samples.

When comparing these results to those in Fig. 1, there is a general increase in transparency for the lignin-containing films, especially those with KL, which showed more significant variation. Lignin, being a polymer, can degrade under prolonged UV exposure, breaking its polymer chains [18]. This reduces particle size within the film and, consequently, decreases opacity, allowing for high light transmission [11]. On the other hand, lignin NP demonstrates superior UV resistance properties, which explains the lesser increase in transparency of the films containing nanoparticles compared to the KL films. This resistance means that films with lignin NP experienced less degradation over the 21-day test, contributing to the maintenance of their opacity.

Furthermore, the addition of lignin in different fractions not only improves the films' UV stability but also effectively blocks photochemical oxidation. The fraction of lignin used influences the balance between transparency and UV protection: lower fractions maintain higher transparency, while higher fractions provide better UV protection but result in increased opacity. This dual functionality of lignin is particularly relevant for sustainable applications, with a growing demand for biodegradable materials that offer UV barrier properties [19].

3.3. Characterization of films before and after UV-C exposure

3.3.1. Structural characterization

FTIR spectra obtained for the PVA films and the MP lignin-added films and their fractions (PVA + KL, PVA + KL30, PVA + KL40 and PVA + KL50, respectively) are shown in Fig. 2A. Based on the spectra, it is possible to observe a similarity between all the samples, which can be attributed to the fact that the films are composed of a large percentage of matrix when compared to the 4 % of additives added. The characteristic bands of PVA and the contributions of the plasticizing agent, glycerol, and lignin are observed. The assignment of the bands is described in detail in SI4.

Although the spectra are generally very similar, it is possible to observe variations in the intensity of the bands at some wavenumbers, such as those in 1711 and 1655 cm^{-1}. This variation suggests structural changes in the matrix due to interaction with the fillers. For pure PVA, there is a higher intensity of the band attributed to CO groups; with the addition of KL, the proportion is reversed, with a greater presence of OH; for fraction 30, this proportion is equal, and for fractions 40 and 50, there is behavior more like pure PVA.

In the spectra presented in Fig. 2B, for the samples after photodegradation, the bands can be seen in the same regions as those present for the samples not exposed to light. However, it is once again possible to see changes in the proportions of some of the bands. When comparing

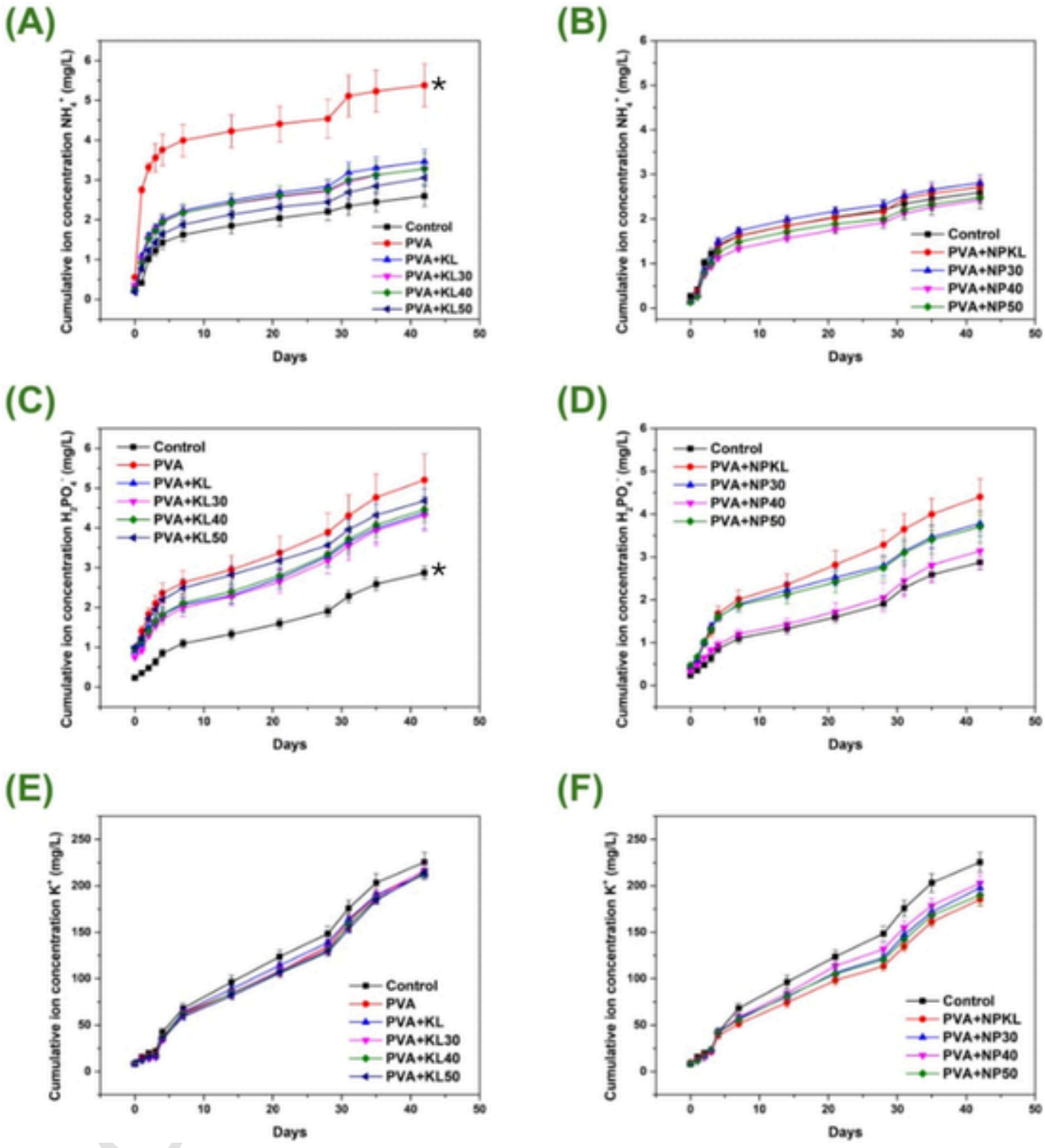

Fig. 7. The curves (A, C, and E) represent the leaching of NH_4^+, K^+, and $H_2PO_4^-$ ions for the PVA and macroparticles fractions, respectively. The curves (B, D, and F) correspond to the leaching of the same ions for the NP fractions, respectively. *Statistically distinct samples.

the spectrum with and without exposure to light, it is possible to observe an increase in the band intensity in the region of 1711 cm^{-1} for all the samples. This region is characteristic of carbonyl groups, which are associated with the photodegradation of polymers in various works in the literature, indicating that the films have undergone modifications with UV-C irradiation. When comparing the photodegraded samples with each other, the only one that did not show a significant increase was PVA + KL, and among the others, the increase was for PVA, followed by those added with the 50, 40, and 30 fractions, which indicates greater photoprotection of the lignin for PVA.

Fig. 2C and D show the spectra for the PVA, PVA + NPKL, PVA + NPKL30, PVA + NPKL40, and PVA + NPKL50 samples, before and after exposure to light, respectively. Bands are observed in the same regions as for the spectra presented above, with slight shifts in

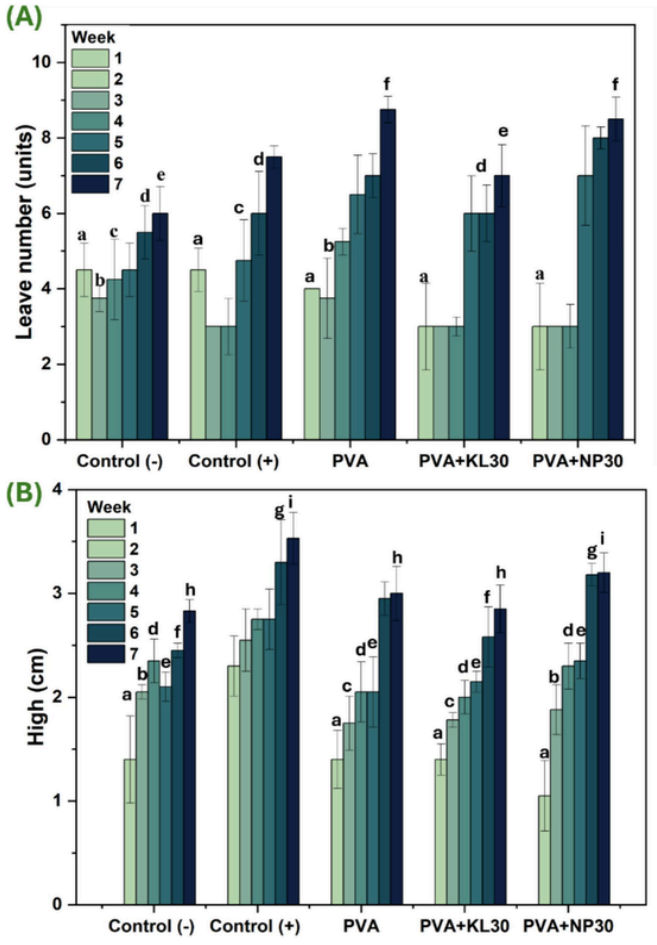

Fig. 8. (A) Number of leaves (units) and (B) seedling height (cm) throughout the experiment for the positive (+) and negative (–) controls, PVA, PVA + KL30, and PVA + NP30 samples. Values represent the mean ± standard deviation of the replicates. [a-i]Statistically similar samples for the same week with different coatings.

the wave numbers. Once again, the region with the change in the proportion of bands when comparing the samples with nanoparticles (Fig. 2C) and without nanoparticles (Fig. 2A), we can see a greater intensity of the characteristic CO band to OH, which for the samples without nanoparticles was very similar. This indicates a modification due to the use of additives in the form of nanoparticles, as there is no such modification for the non-additive PVA. For the set with nanoparticles (Fig. 2 D) there were no significant changes after exposure to light.

3.3.2. *Thermal properties*

The thermogravimetric Analysis (TGA) and first derivative thermogravimetric (DTG) curves of the samples before and after exposure to UV-C light are shown in Fig. 3. Table SI1 shows the results of the thermogravimetric analysis determined by TG and DTG curves. The analyzed parameters included $T_{5\%}$ (onset temperature of degradation with a 5 % mass loss), T_{max} (temperature at the maximum mass loss rate), Δm (mass loss rate until Tmax), and $R_{900°C}$ (carbonaceous residue at 900 °C).

The thermal results of PVA films added with MP and NP lignin reveal how the chemical and structural characteristics of the lignin fractions directly influence the thermal stability and resistance to photooxidative degradation. It was observed that fractions with higher Ph-OH content and lower M_w, such as KL30, provide superior thermal protection (Fig. 3A-B) and photo-stability (Fig. 3C-D). This relationship can be attributed to the high antioxidant capacity of the Ph-OH, which acts as a "radical scavenger" [20,21], slowing down thermal degradation by absorbing radicals and thus protecting the PVA matrix. The most significant values of T5% and Tmax were found for the PVA + KL30 film, which indicates increased initial resistance and maximum stability against thermal degradation and photodegradation (Fig. 3C). In addition, it presents the lowest Δm during heating, which reflects thermal protection, since the antioxidant capacity of Ph-OH slows degradation by heating [22].

KL and the KL50 fraction (Fig. 3A) presented higher Mw values and predominance of aliphatic groups (Aliph-OH) and had the lowest performance in T5% and Tmax. This can be explained by the fact that the majority presence of Aliph-OH, with reduced antioxidant efficacy, suggests a lower capacity to stabilize the matrix against thermal degradation. Since Aliph-OH has reduced efficiency in neutralizing free radicals, KL and the KL50 fraction are less protective and less capable of prolonging the thermal resistance of PVA. Moreover, the higher M_w of these fractions may hinder homogeneous dispersion in the matrix, negatively affecting the film's thermal and UV protection effectiveness. This behavior is reflected by a higher Δm, indicating a more pronounced mass loss during thermal degradation, suggesting lower thermal resistance and stability against UV-C irradiation.

When comparing the same parameter for PVA films additived with lignin NP, it was observed that these films showed better thermal protection performance than lignin and its fractions. However, only the PVA + NP30 film exhibited stability (Fig. 3E). All other treatments underwent degradation due to UV-C irradiation (Fig. 3G), bringing their degradation temperature closer to pure PVA. The addition of nanoparticles was 10 times lower than that of pure lignin, which may indicate that the higher dispersion and the smaller number of nanoparticles were sufficient to provide effective thermal protection. When analyzing the DTG behavior (Fig. 3F), we observed consistency in the performance of the PVA + KL30 film, which showed the highest rate of variation in %·min^{-1} and the highest degradation temperature (indicating resistance), as well as the lowest percentage of mass loss, both before and after UV exposure. When analyzing the treatments with lignin NP, the same behavior was observed for the PVA + NP30 (Fig. 3H) film.

The DSC thermal analysis studied the film's behavior and the chemical interactions between the polymer network and lignin modifications. Fig. 3I shows the thermograms of the various treatments investigated in this work. Within the studied range, the glass transition (T_g) of PVA is marked by an exothermic event, indicating the glass transition at 50 °C [23], where the semicrystalline structure of PVA undergoes a lattice modification. The melting temperature (T_m) is observed at 125 °C [24] as an endothermic event, marking the beginning of material melting. Additionally, a more pronounced endothermic event at 250 °C is seen in all samples, representing the characteristic degradation of PVA. The thermal behavior of PVA and PVA-KL were very similar, likely due to the hydrophobic nature of lignin, which limits its interaction with PVA [25]. On the other hand, the acid treatment that the fractions have undergone improved the interaction between the PVA film and the lignin.

The fractions showed the same glass transition point characteristic of PVA but exhibited different endothermic events [26]. PVA-KL40 showed the least shift, with a peak at 265 °C, compared to PVA and PVA-KL. In contrast, PVA-KL30 and PVA-KL50 displayed a change in the endothermic event, reaching 280 °C. This shift suggests modifications in the film's chemical bonds and, consequently, changes in the material's crystalline structure, which alters the temperature at which the event occurs. Fig. 2K shows the thermograms after UV-C exposure. For all treatments, the glass transition was suppressed. Ultraviolet irradiation damages the polymer structure through chain scission, film crosslinking (reducing chain mobility), and oxidation (chemical degradation). These changes weaken the film, preventing it from undergoing a glass transition since the polymer chains are already compromised [27]. For the endothermic event associated with material degradation,

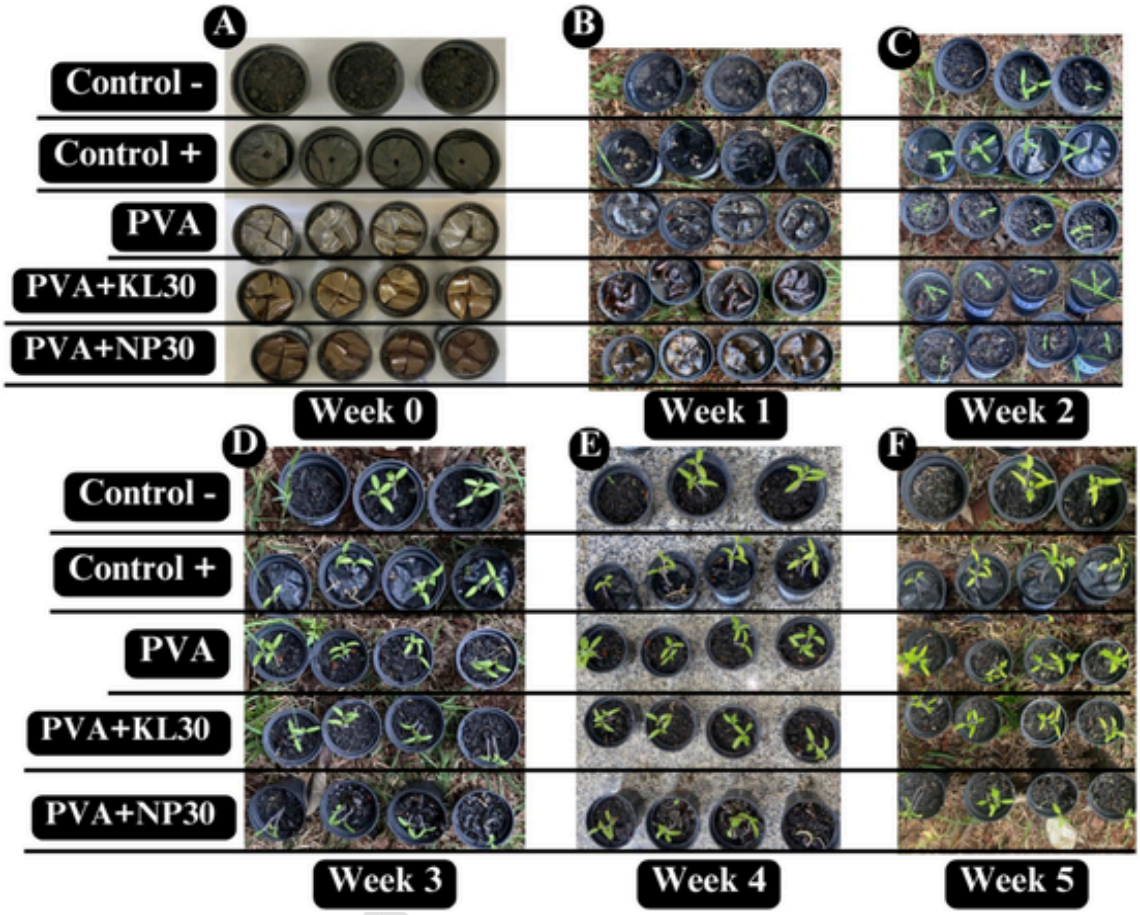

Fig. 9. Photographic records of the monitoring of the degradation of different mulch films, along with plant growth over 5 weeks. (A) Week 0, (B) Week 1, (C) Week 2, (D) Week 3, (E) Week 4, and (F) Week 5. Control - (No film), Control + (Commercial mulch), and coatings with the developed films PVA, PVA + KL30, and PVA + NP30.

all treatments showed temperature shifts near 300 °C, except for PVA and PVA-KL, where the event remained around 265 °C, like the undegraded film. This stability suggests that the lack of interaction between PVA and lignin allowed lignin to shield the polymer matrix from UV degradation [8].

Thus, comparing fractions highlights that the structural characteristics of lignin, such as the content of phenolic groups (Ph-OH) and M_w, are essential for the thermal stabilization of PVA films. Fractions such as KL30, rich in Ph-OH and with lower M_w, provide thermal protection and photo-oxidative resistance. In contrast, fractions with less favorable characteristics, such as KL and KL50, are less effective in providing this protection. This underscores the importance of selecting the appropriate lignin fraction to optimize polymer-based materials' thermal and barrier properties. With reduced Δm and higher T_f, the KL30 fraction proves to be superior in thermal protection and photo-stability, as opposed to fractions with higher molecular weight and aliphatic hydroxyls, which showed higher Δm and lower T_f.

3.3.3. Mechanical properties

Fig. 4 illustrates Young's modulus and elongation at the break of the samples before and after exposure to UV-C radiation. The Young's modulus of the non-photodegraded PVA (Fig. 4A) was 6.5 MPa, a relatively low value attributed to the presence of glycerol, which acts as a plasticizer. Upon the addition of KL, a reduction in Young's modulus was observed compared to the non-photodegraded PVA. This behavior contrasts with findings reported by Gregorich et al. and Xu et al. [28,29]. The reduction in Young's modulus values may be related to the poor miscibility between PVA and KL, as suggested by Kubo and Kadla [30]. The agglomeration of KL particles within the PVA matrix can result in low miscibility, acting as stress concentrators that, in turn, increase the distance between PVA chains, thus reducing intermolecular interactions [31,32].

An increase in Young's modulus values was observed for the samples containing the KL fractions compared to the sample with unfractionated lignin (Fig. 4A). This can be attributed to the increase in hydrogen bonds between the PVA chains and the KL fractions since there is a higher phenolic hydroxyl content in the KL fractions compared to KL [33,34]. Finally, Young's modulus values for all PVA samples with KL fractions (PVA + KL30, PVA + KL40, and PVA + KL50) are statistically like those of pure PVA.

In the case of the PVA + NPKL sample (Fig. 4A), an increase in Young's modulus was observed compared to the PVA + KL samples. This enhancement is attributed to the reduced size of the NPKL particles, which provides a reinforcing effect due to their higher aspect ratio and larger surface area compared to KL particles. These characteristics improve the interaction between NPKL and PVA, facilitating fiber-matrix load transfer and increasing Young's modulus [35].

In Fig. 4B, there was practically no change in comparing Young's modulus values of non-photodegraded PVA (6.52 ± 0.59 MPa) and photodegraded PVA (6.44 ± 1.43 MPa). However, when comparing the PVA + KL and PVA + NPKL samples, the PVA + NPKL samples exhibit higher Young's values. This increase is likely associated with the larger surface area of the NPKL particles, which enhances the interaction between the components (PVA and NPKL). In addition, UV-C expo-

sure induces chemical reactions in vinyl polymers, including the formation of cross-links and internal or terminal double bonds, which contribute to increased composite [36]. UV-C exposure also causes chain scission in PVA, generating free radicals that enhance interactions between kraft lignin particles (KL and NPKL) and the PVA. Consequently, this explains the higher Young's modulus value observed in the PVA + 30, PVA + 40, and PVA + 50 (KL and NPKL fractions) samples compared to non-photodegraded PVA [37].

Fig. 4C illustrates the elongation at break of the non-photodegraded samples. The elongation at break and Young's modulus behavior follows the same trend (Fig. 4A), where the addition of KL resulted in a reduction in elongation at break compared to pure PVA, as also reported by [38]. The reduction can be attributed to the non-uniform distribution of KL particles within the PVA matrix, where the agglomerates create stress concentration points and hinder the sliding of the PVA chains, reducing the film's elongation capacity[35].

The samples with fractionated KL exhibited increased elongation at break values compared to the PVA + KL sample, which can be attributed to the easier sliding of the PVA chains when loaded with KL fractions since the fractionation process reduces the molar mass of KL [33]. An exception was observed for the PVA + KL40, which showed an elongation at a break value nearly identical to pure PVA.

Regarding the PVA + NPKL, Young's modulus values were like those of the PVA + KL samples. Furthermore, when comparing the elongation at break values among the PVA + NPKL samples (PVA + NP30, PVA + NP40, and PVA + NP50), no significant differences were observed, as the values were practically the same across these samples.

Fig. 4D illustrates the elongation at the break of the photodegraded samples. A significant reduction in the elongation capacity of photodegraded PVA is observed, which is attributed to the degradation of the PVA structure. The elongation at the break value of PVA + KL is higher than photodegraded PVA. Moreover, the elongation at break values for the photodegraded PVA + KL, PVA + KL30, PVA + KL40, and PVA + KL50 samples are nearly identical to those of the corresponding non-photodegrade samples (Fig. 4C). This indicates that KL particles effectively shield the PVA structure from photodegradation [39].

A similar protective effect is observed for NPKL particles. However, unlike the PVA + KL samples, all photodegraded PVA + NPKL samples (PVA + NPKL, PVA + NP30, PVA + NP40, and PVA + NP50) exhibit reduced elongation at break values compared to their non-photodegraded counterparts (Fig. 4C). The percentage reductions in elongation at break were approximately 46.3 % (PVA + NPKL), 51.9 % (PVA + NPNP30), 48.9 % (PVA + NP40), and 64.1 % (PVA + NP50). These results suggest that NPKL particles are less effective than KL particles in protecting PVA from UV-C-induced degradation.

A formulation with adequate viscosity, mainly in pseudoplastic materials, ensures uniform application and prevents high spread ability, which can diminish the quality of the film formation. Additionally, the predominance of elastic modulus (G') over viscous modulus (G") indicates dominant elastic behavior, higher structural integrity, and mechanical stability. It is well described that materials with relatively low spreadability and with mechanical resistance can be appropriate to develop structured films. The rheological analysis presents similar results for samples in gel state. As expected for pseudoplastic materials, the viscosity of all gels decreases as the applied frequency increases, a response of the material's structuring to the oscillation (Fig. 5A-B). Solutions containing NP have lower viscosity compared to PVA (Fig. 5A), indicating lower internal organization and lower interaction strength between the solutions' components.

However, the difference is not significant when comparing the S values (Table SI2 – first column), where it is observed that the PVA and PVA-NP solutions present values close to 0.2 Pa.s^n. However, when KL30, KL40, and KL50 are added, the solutions present higher viscosity when compared to the viscosity of PVA, but there is a decrease in the presence of NPKL (Fig. 5B). Furthermore, it is observed that the strength of the gels increases significantly in the presence of KL, KL30 and KL40 ($p < 0.05$), with S between 0.5 Pa.s^n (PVA-KL30 and PVA-KL40) and 0.6 Pa.s^n (PVA -KL) (Table SI2 – first column). In other words, the presence of KL promotes interaction between components of the solutions, which is reflected in the greater viscosity of the materials compared to solutions containing NP [40–42], likely due to strong hydrogen bonds among KL and PVA, as seen in Young's modulus. Although the viscosities are different, the behavior of the elastic modulus variation with frequency is not strongly altered in the presence of the additive, as shown by the n index values between 1.7 and 2.2 (Table SI2 – second column), showing that it prevails the PVA structure as an element that gives elasticity to the system.

3.3.4. Biodegradation

The biodegradation of the samples in soil, as shown in Fig. SI4A, revealed a rapid degradation during the first two days (Fig. SI4B), followed by a slower degradation rate. This behavior can be attributed to the nature of film materials, such as PVA and lignin. The rapid degradation observed at the beginning of the experiment can be attributed to rapid hydrolysis and microbial attack in the most amorphous and hydrophilic regions of the films, since the film is composed of a large part of PVA, which has these characteristics and tends to degrade rapidly because it is highly soluble in water [43].

The rate of evolution of the degradation process was reduced after the first two days (Fig. SI4C), probably indicating that the more crystalline and less accessible regions of the material began to be exposed; these regions are generally more resistant to microbial attack [44]. Lignin can also contribute to this slowdown due to its complex structure, resistance to biodegradation, and can be a barrier to water penetration and microbial activity [29].

After one month (Fig. SI4D), all samples exhibited similar degradation patterns, suggesting relatively uniform behavior among the different films, regardless of variations in their formulations. This indicates that while adding a lignin alters the films' initial properties, such as solubility and resistance, the impact on long-term biodegradability in soil is not significantly differentiated. Similarly, a result was obtained for nanoparticle samples (Fig. SI5). It was observed that after one month, compared to the samples without nanoparticles, there was a slightly faster biodegradation, which was expected given that they are nanoparticles.

The results of accelerated biodegradation in soil are presented in Fig. 6. For the samples without nanoparticles (6A and 6B), a continuous increase in daily CO_2 release is observed, with the PVA + KL50 sample initially showing the highest values, reaching approximately 60 mg of CO_2. However, this behavior changes over time, as the PVA + KL30 sample exhibits higher release levels from day 16 onward, reaching about 90 mg of CO_2. In the formulations containing nanoparticles (6C and 6D), the PVA + NP40 and PVA + NP50 samples stand out with the highest cumulative CO_2 release values, suggesting increased microbial accessibility promoted by the nanoparticles. This trend is further supported by the linear fittings applied to the daily CO_2 release data (Figs. SI6 and SI7), with the highest slopes observed for PVA + NP40 (3.00 mg/day; $R^2 = 0.95$) and PVA + NP50 (2.89 mg/day; $R^2 = 0.98$), indicating superior biodegradation rates compared to the other formulations.

3.3.5. Leaching of NH_4^+, $H_2PO_4^-$, and K^+ ions

The ion leaching analysis was conducted over 42 days. Due to the high degradability of PVA, daily measurements were performed until the fourth day, followed by weekly collections, with an additional measurement on day 31, near the end of soil biodegradation (Fig. SI4 and SI5). For better visualization, the graphs were divided based on the

presence of macroparticles (Fig. 7A, C, and E) or nanoparticles (Fig. 7B, D, and F) for NH_4^+, K^+, and $H_2PO_4^-$ ions, respectively. Commercial NPK in the soil was included in both sets for comparison.

At the beginning of the experiment, the PVA samples exhibited the highest fertilizer release rates for NH_4^+ and $H_2PO_4^-$ ions (Fig. 7 A and B), which can be attributed to the structural fragility of PVA, as widely documented in the literature [5,6,45]. The fragility of PVA facilitates the rapid degradation of the polymeric matrix, resulting in a more immediate and substantial release of macronutrients. This behavior suggests that formulations with PVA undergo accelerated degradation, allowing for a more pronounced initial nutrient release. On the other hand, the films containing NP (Fig. 7B, D, and F) showed low nutrient release at the experiment. This indicates better stability of these films, delaying degradation and gradually releasing NPK fertilizer ions.

The different release profiles between the films with MP and NP show that NP can increase the polymer matrix's resistance to degradation and generate a more controlled release of ions. The PVA sample without lignin may have undergone greater microbial activity [46], accelerating film degradation and increasing nutrient release.

The antibacterial properties of lignin [47,48] can also modulate the microbial activity of films, especially those containing NP, due to the greater surface area and homogeneity of dispersion with MP. This inhibits the proliferation of microorganisms that could accelerate the degradation of films and the release of nutrients. Finally, films with NP presented a more controlled release of nutrients than those with MP and PVA.

To further clarify the kinetics of nutrient release, Table SI3 presents the calculated slopes for each nutrient during the early and sustained leaching phases. These values highlight distinct degradation behaviors among the formulations. PVA-based films, particularly neat PVA and PVA + KL, exhibited the highest initial release rates for NH_4^+ (0.335 and 0.597 mg L^1 day^1, respectively), confirming their rapid disintegration. In contrast, formulations containing nanoparticles, especially PVA + NP40 and PVA + NP50, showed significantly lower early-phase slopes ($\leq$ 0.19 mg L^{-1} day^{-1}), consistent with a more gradual and controlled nutrient release. For $H_2PO_4^-$, the early-phase release was again higher in PVA and PVA + KL (−0.269 and − 0.251 mg L^{-1} day^{-1}, respectively), whereas the NP-containing films displayed reduced and sustained release, with negligible slopes in the second phase. These results support the hypothesis that NP improves film stability and modulates nutrient release by delaying polymer degradation and mitigating microbial activity.

3.4. Application of mulch film for tomato cultivation

Mulch films are widely used in agriculture as surface soil coverings, playing a crucial role in moisture conservation, weed control, and soil temperature regulation. Additionally, these films can act as a physical barrier, reducing erosion and minimizing the leaching of essential nutrients. Incorporating biodegradable materials, such as lignin and PVA, in the formulation of these films has been a promising strategy to combine agronomic efficiency with environmental sustainability, reducing the impact of plastic waste accumulation in agricultural fields.

The results indicate that seedling height (Fig. 8A) and the emergence of the first leaves (Fig. 8B) occurred from the second week in all tested conditions. During the first weeks, the control samples presented the best results. The negative control (No cover) may have allowed greater gas exchange and direct absorption of sunlight, facilitating seedling emergence. On the other hand, positive control (Commercial) may have helped stabilize these initial conditions, promoting uniform growth. In the following weeks (3 and 4), negative control presented the highest number of leaves compared to the other treatments. This result may be associated with the absence of physical barriers in the soil, allowing oxygen and light availability during the early growth stages. However, from the fifth week onwards, all films have already degraded except the positive control, commercial mulch, Fig. 9. The samples containing mulch films began to perform better than the negative control. This can be attributed to reduced soil water evaporation, providing a more favorable plant growth environment. This is attributed to the moisture retained [49] by commercial films and the residual PVA-based films that may still act in this way, even though they are not visually apparent, since by the fifth week onwards, the films appear to have been completely degraded (Figs. SI4 and SI5).

Regarding plant height, the positive control (+) with the commercial mulch film showed the best results throughout the experiment (Fig. 9B), demonstrating its effectiveness in soil protection and plant growth optimization. However, in the final weeks, the PVA + NP30 film achieved statistically similar results to the positive control, suggesting that lignin nanoparticles significantly contributed to plant development. This can be explained by the ability of nanoparticulated lignin to act as a photodegradation protector, providing better film stability over time and reducing thermal degradation of the mulch layer [50]. Lignin nanoparticles have a greater capacity to absorb part of the UV radiation, thus minimizing environmental stress and promoting better plant development. The other films developed (PVA and PVA + KL30) showed intermediate performance but were superior to the negative control in the final weeks of the experiment. This result reinforces the importance of mulch films in regulating the soil microclimate [51]. These findings highlight the relevance of biodegradable mulch films in sustainable agriculture, as they not only provide soil protection and moisture control but also demonstrate the potential of lignin nanoparticle-based films as a promising alternative to partially replace commercial mulch films, reducing environmental impact and promoting more efficient crop growth [52].

4. Conclusion

This study demonstrated that incorporating KL and its fractions, in both macroparticulate and nanoparticulate forms, significantly enhanced the properties of PVA films, particularly regarding UV resistance, thermal stability, and biodegradability. Nanoparticulated lignin improved UV protection, reducing transparency loss, while the KL30 fraction provided superior thermal and photostability. Rheological analysis confirmed Newtonian behavior with low hysteresis, and biodegradation assays indicated slightly faster degradation for nanoparticle-containing films due to their higher surface area. The application of these films as mulch for cherry tomato cultivation confirmed their benefits for soil protection and plant growth. The best results were initially observed for the commercial mulch (+) and uncovered soil (−) controls. However, lignin films improved moisture retention from the fifth week onwards and created more stable growth conditions. Ultimately, the PVA + NP30 film matched the performance of the commercial mulch, likely due to the photoprotective effect of lignin nanoparticles. The PVA and PVA + KL30 films also surpassed the negative control toward the end of the cultivation period, confirming their effectiveness in soil microclimate regulation. These findings highlight lignin-based mulch films as a sustainable alternative to commercial mulches, enhancing soil protection, plant development, and controlled nutrient release.

CRediT authorship contribution statement

Amanda S.M. de Freitas: Writing – original draft, Project administration, Methodology, Investigation, Formal analysis, Conceptualization. **Jéssica S. Rodrigues:** Writing – original draft, Project administration, Methodology, Investigation, Formal analysis, Conceptualization. **Lucas V.B. Fré:** Writing – original draft, Investigation. **Henrique O.S. Vieira:** Writing – original draft, Investigation. **Maria E.S. Nascimento:** Writing – original draft, Investigation. **Stefanny F. Amaro:** Writing – original draft, Investigation. **Livia S. Emidio:**

Writing – original draft, Investigation. **Daniele R. de Araujo:** Writing – original draft, Investigation. **Anderson F. Sepulveda:** Writing – original draft, Investigation. **Daniel Komatsu:** Writing – original draft, Investigation. **Vagner R. Botaro:** Writing – review & editing, Supervision, Funding acquisition. **Leonardo F. Fraceto:** Writing – review & editing, Supervision, Funding acquisition. **Marystela Ferreira:** Writing – review & editing, Supervision, Funding acquisition.

Declaration of competing interest

The authors declare that they have no known competing financial interests or personal relationships that could have appeared to influence the work reported in this paper.

Acknowledgments

This research was partially funded by the São Paulo State Research Support Foundation (FAPESP) through grants #2023/06505-9 (M.F.), #2024/01872-6 (L.F.), #2024/14149-0 (A.F), #2023/00335-4 (J.R), and CEPID CBioClima #2021/10639-5. Also the project 14805 – FINEP 01.22.0179.00 (MARTMA), as well as by the National Council for Scientific and Technological Development (CNPq) through grant #153850/2024-8 and the INCT Nanotechnology for Sustainable Agriculture program (MCTI-CNPq - INCTNanoAgro #405924/2022-4) and Coordenação de Aperfeiçoamento de Pessoal de Nível Superior – Brasil (CAPES-MEC INCTNanoAgro #88887.953443/2024-00). And the National Institute of Science and Technology in Organic Electronics (INEO). Also, the authors would like to thank the Biorender platform for providing the tool that facilitated the design of the figures.

Data availability

Data will be made available on request.

Appendix A. Supplementary data

Supplementary data to this article can be found online at https://doi.org/10.1016/j.ijbiomac.2025.144386.

References

[1] F.N. Eze, R.C. Eze, S. Singh, K.E. Okpara, Fabrication of a versatile and efficient ultraviolet blocking biodegradable composite film consisting of Tara gum/PVA/Riceberry phenolics reinforced with biogenic riceberry phenolic-rich extract-nanosilver, Int. J. Biol. Macromol. 278 (2024) 134914, https://doi.org/10.1016/j.ijbiomac.2024.134914.

[2] P. Threepopnatkul, P. Thongloy, W. Janpromdee, S. Utamachote, S. Phattarateera, Effect of fruit peel extracts on properties of PVA composites films for agricultural applications, Mater. Today Proc. 47 (2021) 3560–3564, https://doi.org/10.1016/j.matpr.2021.03.560.

[3] W. Zhang, A. Khan, P. Ezati, R. Priyadarshi, M.A. Sani, N.B. Rathod, G. Goksen, J.-W. Rhim, Advances in sustainable food packaging applications of chitosan/polyvinyl alcohol blend films, Food Chem. 443 (2024) 138506, https://doi.org/10.1016/j.foodchem.2024.138506.

[4] H. Shekaryar, S. Norouzbahari, A review on versatile applications of polyvinyl alcohol thin films, specifically as sensor devices, Polym. Eng. Sci. 64 (2024) 455–468, https://doi.org/10.1002/pen.26569.

[5] M. Ismayati, N.A.N. Fatah, E.E. Ernawati, Juliandri, W.B. Kusumaningrum, M.A.R. Lubis, W. Fatriasari, N.N. Solihat, F.P. Sari, A. Halim, I.A. Cholilie, Y. Tobimatsu, Antioxidant and uv-blocking activity of PVA/tannin-based bioplastics in food packaging application, Int. J. Biol. Macromol. 257 (2024) 128332, https://doi.org/10.1016/j.ijbiomac.2023.128332.

[6] G.S.A. Suleiman, X. Zeng, R. Chakma, I.Y. Wakai, Y. Feng, Recent advances and challenges in thermal stability of PVA –based film: a review, Polym. Adv. Technol. 35 (2024), https://doi.org/10.1002/pat.6327.

[7] M. Parit, P. Saha, V.A. Davis, Z. Jiang, Transparent and homogenous cellulose nanocrystal/lignin UV-protection films, ACS Omega 3 (2018) 10679–10691, https://doi.org/10.1021/acsomega.8b01345.

[8] H. Sadeghifar, A. Ragauskas, Lignin as a UV light blocker—a review, Polymers (Basel) 12 (2020) 1134, https://doi.org/10.3390/polym12051134.

[9] V. Girard, H. Chapuis, N. Brosse, N. Canilho, L. Marchal-Heussler, I. Ziegler-Devin, Lignin nanoparticles: contribution of biomass types and fractionation for an eco-friendly production, ACS Sustain. Chem. Eng. 12 (2024) 7055–7068, https://doi.org/10.1021/acssuschemeng.4c00711.

[10] Jéssica S. Rodrigues, V. Lima, L.C.P. Araújo, V.R. Botaro, Lignin fractionation methods: can lignin fractions be separated in a true industrial process? Ind. Eng. Chem. Res. 60 (2021) 10863–10881, https://doi.org/10.1021/acs.iecr.1c01704.

[11] J.S. Rodrigues, A. de S.M. de Freitas, H.S.M. Lopes, A.A.F. Pires, A.P. Lemes, M. Ferreira, V.R. Botaro, Improvement of UV stability of thermoplastic starch matrix by addition of selected lignin fraction - photooxidative degradation, Int. J. Biol. Macromol. 230 (2023) 123142, https://doi.org/10.1016/J.IJBIOMAC.2023.123142.

[12] A. do E.S. Pereira, J. Luiz de Oliveira, S. Maira Savassa, C. Barbara Rogério, G. Araujo de Medeiros, L.F. Fraceto, Lignin nanoparticles: new insights for a sustainable agriculture, J. Clean. Prod. 345 (2022) 131145, https://doi.org/10.1016/J.JCLEPRO.2022.131145.

[13] M. Morsali, A. Moreno, A. Loukovitou, I. Pylypchuk, M.H. Sipponen, Stabilized lignin nanoparticles for versatile hybrid and functional nanomaterials, Biomacromolecules 23 (2022) 4597–4606, https://doi.org/10.1021/acs.biomac.2c00840.

[14] N. Gontard, S. Guilbert, J. Cuq, Edible wheat gluten films: influence of the main process variables on film properties using response surface methodology, J. Food Sci. 57 (1992) 190–195, https://doi.org/10.1111/j.1365-2621.1992.tb05453.x.

[15] N.I.F. Himmah, G. Djajakirana, D. Darmawan, Nutrient release performance of starch coated NPK fertilizers and their effects on corn growth, SAINS TANAH - Journal of Soil Science and Agroclimatology 15 (2018) 104, https://doi.org/10.15608/stjssa.v15i2.19694.

[16] Q. Tang, Y. Qian, D. Yang, X. Qiu, Y. Qin, M. Zhou, Lignin-based nanoparticles: a review on their preparations and applications, Polymers 12 (2020) 2471, https://doi.org/10.3390/POLYM12112471.

[17] X. Li, Y. Liu, X. Ren, Transparent and ultra-tough PVA/alkaline lignin films with UV shielding and antibacterial functions, Int. J. Biol. Macromol. 216 (2022) 86–94, https://doi.org/10.1016/J.IJBIOMAC.2022.06.188.

[18] H.A. Carter, The chemistry of paper preservation: part 1. The aging of paper and conservation techniques, J. Chem. Educ. 73 (1996) 417, https://doi.org/10.1021/ed073p417.

[19] W. Yang, H. Ding, G. Qi, C. Li, P. Xu, T. Zheng, X. Zhu, J.M. Kenny, D. Puglia, P. Ma, Highly transparent PVA/nanolignin composite films with excellent UV shielding, antibacterial and antioxidant performance, React. Funct. Polym. 162 (2021) 104873, https://doi.org/10.1016/j.reactfunctpolym.2021.104873.

[20] J.M. Jardim, P.W. Hart, L. Lucia, H. Jameel, Insights into the potential of hardwood Kraft lignin to be a green platform material for emergence of the biorefinery, Polymers (Basel) 12 (2020) 1795, https://doi.org/10.3390/polym12081795.

[21] X. Zhang, Weifeng Liu, Wenqiang Liu, X. Qiu, High performance PVA/lignin nanocomposite films with excellent water vapor barrier and UV-shielding properties, Int. J. Biol. Macromol. 142 (2020) 551–558, https://doi.org/10.1016/j.ijbiomac.2019.09.129.

[22] J. Zhang, Z. Tian, X. Ji, F. Zhang, Fabrication mechanisms of lignin nanoparticles and their ultraviolet protection ability in PVA composite film, Polymers (Basel) 14 (2022) 4196, https://doi.org/10.3390/polym14194196.

[23] F. Reguieg, L. Ricci, N. Bouyacoub, M. Belbachir, M. Bertoldo, Thermal characterization by DSC and TGA analyses of PVA hydrogels with organic and sodium MMT, Polym. Bull. 77 (2020) 929–948, https://doi.org/10.1007/s00289-019-02782-3.

[24] M. Parit, H. Du, X. Zhang, Z. Jiang, Flexible, transparent, UV-protecting, water-resistant nanocomposite films based on polyvinyl alcohol and Kraft lignin-grafted cellulose nanofibers, ACS Appl. Polym. Mater. 4 (2022) 3587–3597, https://doi.org/10.1021/acsapm.2c00157.

[25] A. Eraghi Kazzaz, P. Fatehi, Interaction of synthetic and lignin-based sulfonated polymers with hydrophilic, hydrophobic, and charged self-assembled monolayers, RSC Adv. 10 (2020) 36778–36793, https://doi.org/10.1039/D0RA07554J.

[26] D.M. Fernandes, A.A. Winkler Hechenleitner, A.E. Job, E. Radovanocic, E.A. Gómez Pineda, Thermal and photochemical stability of poly(vinyl alcohol)/modified lignin blends, Polym. Degrad. Stab. 91 (2006) 1192–1201, https://doi.org/10.1016/j.polymdegradstab.2005.05.024.

[27] Y. Lei, L. Mao, J. Yao, H. Zhu, Improved mechanical, antibacterial and UV barrier properties of catechol-functionalized chitosan/polyvinyl alcohol biodegradable composites for active food packaging, Carbohydr. Polym. 264 (2021) 117997, https://doi.org/10.1016/j.carbpol.2021.117997.

[28] N. Gregorich, S. Kanhere, J. Stutts, K. Bethel, G. Tindall, B. Lynn, A.A. Ogale, M.C. Thies, E.M. Davis, Enhanced mechanical properties of composite hydrogels containing fractionated and purified lignin, ACS Appl Polym Mater 5 (2023) 201–213, https://doi.org/10.1021/acsapm.2c01433.

[29] Y.-H. Xu, M.-F. Li, F. Peng, Lignin micro/nanoparticles: synthesis, properties, and application to endow polyvinyl alcohol film with multi-functionality, Chem. Eng. J. 473 (2023) 145233, https://doi.org/10.1016/j.cej.2023.145233.

[30] S. Kubo, J.F. Kadla, The formation of strong intermolecular interactions in immiscible blends of poly(vinyl alcohol) (PVA) and lignin, Biomacromolecules 4 (2003) 561–567, https://doi.org/10.1021/bm025727p.

[31] M.H. Ramadhan, A. Nurrahman, S. Steven, Y. Mardiyati, Enhancing mechanical properties, degradation rate, and water resistance of bioplastic Lignin/Polyvinyl Alcohol (PVA) by fractionation of lignin, Emerg. Mater. (2024), https://doi.org/10.1007/s42247-024-00805-y.

[32] P. Rejmontová, A. Kovalcik, P. Humpolíček, Z. Capáková, E. Wrzecionko, P. Sáha, The use of fractionated Kraft lignin to improve the mechanical and biological properties of PVA-based scaffolds, RSC Adv. 9 (2019) 12346–12353, https://doi.org/10.1039/C8RA09757G.

[33] M. Alekhina, O. Ershova, A. Ebert, S. Heikkinen, H. Sixta, Softwood Kraft lignin

for value-added applications: fractionation and structural characterization, Ind. Crop. Prod. 66 (2015) 220–228, https://doi.org/10.1016/j.indcrop.2014.12.021.
[34] V.A.C. Monteiro, K.T. da Silva, L.R.R. da Silva, A.L.A. Mattos, R.M. de Freitas, S.E. Mazzetto, D. Lomonaco, F. Avelino, Selective acid precipitation of Kraft lignin: a tool for tailored biobased additives for enhancing PVA films properties for packaging applications, React. Funct. Polym. 166 (2021) 104980, https://doi.org/10.1016/j.reactfunctpolym.2021.104980.
[35] E. Espinosa, I. Bascón-Villegas, A. Rosal, F. Pérez-Rodríguez, G. Chinga-Carrasco, A. Rodríguez, PVA/(ligno)nanocellulose biocomposite films. Effect of residual lignin content on structural, mechanical, barrier and antioxidant properties, Int. J. Biol. Macromol. 141 (2019) 197–206, https://doi.org/10.1016/j.ijbiomac.2019.08.262.
[36] A. Bozdoğan, B. Aksakal, O. Yargi, U. Şahintürk, Structural and tensile characteristics of reduced graphene oxide/poly (vinyl alcohol) composite films: influence of ultraviolet irradiation, Polym. Compos. 41 (2020) 3087–3100, https://doi.org/10.1002/pc.25600.
[37] M.L. Pourciel, J. Launay, W. Sant, V. Conédéra, A. Martinez, P. Temple-Boyer, Development of photo-polymerisable polyvinyl alcohol for biotechnological applications, Sens. Actuators B Chem. 94 (2003) 330–336, https://doi.org/10.1016/S0925-4005(03)00463-5.
[38] P. Posoknistakul, C. Tangkrakul, P. Chaosuanphae, S. Deepentham, W. Techasawong, N. Phonphirunrot, S. Bairak, C. Sakdaronnarong, N. Laosiripojana, Fabrication and characterization of lignin particles and their ultraviolet protection ability in PVA composite film, ACS Omega 5 (2020) 20976–20982, https://doi.org/10.1021/acsomega.0c02443.
[39] D. Piccinino, E. Capecchi, V. Trifero, E. Tomaino, C. Marconi, A. Del Giudice, L. Galantini, S. Poponi, A. Ruggieri, R. Saladino, Lignin nanoparticles as sustainable photoprotective carriers for sunscreen filters, ACS Omega 7 (2022) 37070–37077, https://doi.org/10.1021/acsomega.2c02133.
[40] A.F. Sepulveda, M. Kumpgdee-Vollrath, M.K.K.D. Franco, F. Yokaichiya, D.R. de Araujo, Supramolecular structure organization and rheological properties modulate the performance of hyaluronic acid-loaded thermosensitive hydrogels as drug-delivery systems, J. Colloid Interface Sci. 630 (2023) 328–340, https://doi.org/10.1016/j.jcis.2022.10.064.
[41] X. Sun, F. Pei, Y. Fang, The effects of hydrocolloids on the thermomechanical, viscoelastic and microstructural properties of whole wheat flour dough, Food Chem. 370 (2022) 130976, https://doi.org/10.1016/j.foodchem.2021.130976.
[42] F.D. Victorelli, G.M.F. Calixto, M.A.D.S. Ramos, T.M. Bauab, M. Chorilli, Metronidazole-loaded polyethyleneimine and chitosan-based liquid crystalline system for treatment of staphylococcal skin infections, J. Biomed. Nanotechnol. 14 (2018) 227–237, https://doi.org/10.1166/jbn.2018.2484.
[43] J. Yan, M. Li, H. Wang, X. Lian, Y. Fan, Z. Xie, B. Niu, W. Li, Preparation and property studies of chitosan-PVA biodegradable antibacterial multilayer films doped with Cu2O and nano-chitosan composites, Food Control 126 (2021) 108049, https://doi.org/10.1016/j.foodcont.2021.108049.
[44] A. De Campos, J.C. Marconato, S.M. Martins-Franchetti, Biodegradation of blend films PVA/PVC, PVA/PCL in soil and soil with landfill leachate, Arch. Biol. Technol. v 54 (2011) 1367–1378.
[45] W. Zhang, A. Khan, P. Ezati, R. Priyadarshi, M.A. Sani, N.B. Rathod, G. Goksen, J.-W. Rhim, Advances in sustainable food packaging applications of chitosan/polyvinyl alcohol blend films, Food Chem. 443 (2024) 138506, https://doi.org/10.1016/j.foodchem.2024.138506.
[46] L.Y. Stein, M.G. Klotz, The nitrogen cycle, Curr. Biol. 26 (2016) R94–R98, https://doi.org/10.1016/j.cub.2015.12.021.
[47] A. Alzagameem, S.E. Klein, M. Bergs, X.T. Do, I. Korte, S. Dohlen, C. Hüwe, J. Kreyenschmidt, B. Kamm, M. Larkins, M. Schulze, Antimicrobial activity of lignin and lignin-derived cellulose and chitosan composites against selected pathogenic and spoilage microorganisms, Polymers (Basel) 11 (2019) 670, https://doi.org/10.3390/polym11040670.
[48] K. Li, W. Zhong, P. Li, J. Ren, K. Jiang, W. Wu, Antibacterial mechanism of lignin and lignin-based antimicrobial materials in different fields, Int. J. Biol. Macromol. 252 (2023) 126281, https://doi.org/10.1016/j.ijbiomac.2023.126281.
[49] K. Sirivechphongkul, N. Chiarasumran, M. Saisriyoot, A. Thanapimmetha, P. Srinophakun, K. Iamsaard, Y.-T. Lin, Agri-biodegradable mulch films derived from lignin in empty fruit bunches, Catalysts 12 (2022) 1150, https://doi.org/10.3390/catal12101150.
[50] Z. Huang, Y. Zhang, C. Zhang, F. Yuan, H. Gao, Q. Li, Lignin-based composite film and its application for agricultural mulching, Polymers (Basel) 16 (2024) 2488, https://doi.org/10.3390/polym16172488.
[51] R.A. de França, A.C.F. dos S. Rosa, C.J. de F. Braz, R. Barbosa, T.S. Alves, Development of mulch films from biodegradable polymer and agro-industrial waste, Polímeros 34 (1) (2024) e20230042, https://doi.org/10.1590/0104-1428.20230043.
[52] Z. Sun, J. Liang, M. Qin, R. Ning, X. Liu, W. Sun, X. Li, Fabrication of modified lignin-based liquid mulching film and its potential application, Nord. Pulp Paper Res. J. 39 (2024) 201–211, https://doi.org/10.1515/npprj-2023-0071.
[53] J. S. Rodrigues, A. S. M. de Freitas, V. R. Botaro, M. Ferreira, L. F. Fraceto, Tailoring kraft lignin for high-performance nanoparticles: from structure to function,International, Journal of Biological Macromolecules 312 (2025) 144181. https://doi.org/10.1016/j.ijbiomac.2025.144181.